[F-18]-Fluoro-2-deoxy-D-glucose positron emission tomography as a tool for early detection of immunotherapy response in a murine B cell lymphoma model.

Coralie Chaise, Emmanuel Itti, Yolande Petegnief, Evelyne Wirquin, Christiane Copie-Bergman, Jean-Pierre Farcet, Marie-Hélène Delfau-Larue, Michel Meignan, Jean-Noël Talbot, Valérie Molinier-Frenkel

Cancer Immunology and Immunotherapy 08/2007; 56(8): 1163-71

[F-18]-Fluoro-2-deoxy-D-glucose positron emission tomography as a tool for early detection of immunotherapy response in a murine B-cell lymphoma model

Coralie Chaise[1,2], Emmanuel Itti[2,3], Yolande Petegnief[4], Evelyne Wirquin[2,3], Christiane Copie-Bergman[1,2,5], Jean-Pierre Farcet[1,2,6], Marie-Hélène Delfau-Larue[1,2,6], Michel Meignan[2,3], Jean-Noël Talbot[4] and Valérie Molinier-Frenkel[1,2,6]*

[1]INSERM, U617, Créteil, F-94000 France; [2]Université Paris 12, Faculté de Médecine, Créteil, F-94000 France; [3]AP-HP, Hôpital Henri Mondor, Service de Médecine Nucléaire, Créteil, F-94000 France; [4]AP-HP, Hôpital Tenon, Service de Biophysique, Paris, France ; [5]AP-HP, Hôpital Henri Mondor, Département de Pathologie, Créteil, F-94000 France, and [6]AP-HP, Hôpital Henri Mondor, Service d'Immunologie Biologique, Créteil, F-94000 France.

C Chaise and E Itti contributed equally to the work

* Corresponding author. Address: Service d'Immunologie Biologique, Hôpital Henri Mondor, 51 av du Maréchal de Lattre de Tassigny, 94010 Créteil cedex, France.
Phone: (33)1 49 81 48 89. Fax: (33)1 49 81 28 97. e-mail: frenkel@im3.inserm.fr.

Running title: Murine lymphoma monitoring by FDG-PET

Abstract

[F-18]-fluoro-2-deoxy-D-glucose positron emission tomography (FDG-PET) is a non-invasive imaging technique which has recently been validated for the assessment of therapy response in patients with aggressive non-Hodgkin's lymphoma. Our objective was to determine its value for the evaluation of immunotherapy efficacy in immunocompetent Balb/c mice injected with the A20 syngeneic B lymphoma cell line. The high level of *in vitro* FDG uptake by A20 cells validated the model for further imaging studies. When injected intravenously, the tumour developed as nodular lesions mostly in liver and spleen, thus mimicking the natural course of an aggressive human lymphoma. FDG-PET provided three-dimensionnal images of tumour extension including non palpable lesions, in good correlation with *ex-vivo* macroscopic examination. When mice were pre-immunized with an A20 cell lysate in adjuvant before tumour challenge, their significantly longer survival, compared to control mice, was associated with a lower incidence of lymphoma visualized by PET at different time points. Estimation of tumour growth and metabolism using the calculated tumour volumes and maximum standardized uptake values respectively, also demonstrated delayed lymphoma development and lower activity in the vaccinated mice. Thus, FDG-PET is a sensitive tool relevant for early detection and follow-up of internal tumours, allowing discrimination between treated and non-treated small animal cohorts without invasive intervention.

Key words: FDG, PET, small animal imaging, lymphoma

Introduction

Imaging of tumour cells using [F-18]-fluoro-2-deoxy-D-glucose positron emission tomography (FDG-PET) plays an increasing role in oncology, particularly for the assessment of therapy response in aggressive non-Hodgkin's lymphoma [1, 2]. Indeed, FDG-PET helps to clarify the status of residual masses of uncertain fibrotic or malignant nature and allows the reclassification of up to 50% of patients with lymphoma previously considered to be partial responders by conventional imaging as complete responders [3]. The success of this molecular imaging technique relies on the fact that most malignant cells demonstrate increased glycolysis and glucose transporter expression (GLUT 1 and 3) because of their high energy demand for proliferation [4, 5]. The radiotracer FDG is a glucose analogue in which the hydroxyl group in position 2 has been replaced by a positron-emitting atom of fluorine 18 [6]. Similar to glucose, FDG is avidly captured by tumour cells but gets entrapped since, after initial phosphorylation by the hexokinase, it can neither undergo further glycolytic reaction nor exit the cells by dephosphorylation due to lower glucose-6-phosphatase levels [7]. Routinely used in humans [8], the FDG-PET technique has recently benefited from improvement in positron detection systems, allowing the development of high resolution devices for small animals, referred to as "micro PET" systems [9, 10].

The A20 mouse model of lymphoma has been widely used for the preclinical *in vivo* evaluation of immunotherapy against lymphoma [11-18]. When cells are transferred to the mouse by intravenous route, tumour development indeed resembles the natural course of an aggressive human lymphoma with progressive invasion of the spleen, lymph nodes and bone marrow [12, 19]. However, evaluation of the efficacy of the vaccination procedure relies on survival monitoring which is not perfectly correlated with disease development and does not conform to the current recommendations for laboratory animal care [12, 18].

The purpose of the present work was to evaluate the feasibility and relevance of A20 tumour growth monitoring using FDG and micro PET in a prospective cohort of syngeneic and immunocompetent Balb/c mice. Our model was designed to further demonstrate the value of FDG-PET for the objective measurement of the anti-tumour effect induced by a tumour-specific vaccination procedure.

Materials and Methods:

Mice and cell lines

Immunocompetent female Balb/c mice were purchased from Janvier (Le-Genest-Saint-Isle, France). Experiments were conducted with animals from 8 to 12 weeks of age. Mice were maintained in accordance with institutional guidelines. The A20 B-cell lymphoma line and the P815 mastocytoma cell line, both derived from Balb/c mice, were obtained from the American type culture collection (ATCC, LGC promochem, Molsheim, France) and grown *in vitro* in classical RPMI medium (RPMI 1640, 100 U/ml of penicillin, 100 µg/ml of streptomycin, 50 µM β-mercaptoethanol) supplemented with 10% fetal calf serum (PAA Laboratories Ltd, Yeovil, United Kingdom).

In vitro assessment of FDG uptake by A20 cells

FDG uptake was measured in A20 cells and control splenocytes from healthy Balb/c mice to ensure the validity of the A20 lymphoma model for further imaging. Cells were washed twice in phosphate buffer saline (PBS) and resuspended at 5×10^6/ml in PBS alone or in PBS supplemented with 0.8 g/l competitor glucose as indicated. For each cell/media combination, 10^6 cells each incubated in triplicate with 3.7 MBq FDG (250 µl final volume) at 37°C for 10, 40, 60 and 120 min. At the end of each incubation period, the cells were spun down by centrifugation and radioactivity in the cell pellet and supernatant was measured during 30 s using a well gamma counter equipped with a 3-inch crystal. Results were expressed as follows: *% FDG uptake = cell pellet counts/[cell pellet + supernatant counts]* (Eq. 1).

Tumour injection experiments

For intravenous tumour injection experiments, live A20 cells (10^5 per mouse) were washed twice, resuspended in PBS and injected through the tail vein. Mice were examined daily for detection of palpable tumour or death and were eventually sacrificed when external signs of suffering were present (such as reduced mobility and altered behaviour). Two prospective cohorts were conducted for PET-monitoring validation. A first cohort of 10 mice was followed by FDG-PET imaging at day 42 (when two mice displayed the first clinical signs of tumour invasion) and day 49 after tumour injection. All mice were sacrificed at day 50 to examine macroscopic aspect of the lesions and to correlate the foci of uptake with the presence of tumours. Secondly, two cohorts of mice were challenged simultaneously, but one cohort (VAC, *n=7*) had been immunized 5 days prior to challenge with an A20 cell-specific vaccine (see below) while the other (NI, *n=8*) was not immunized and served as a control for

tumour development. The two cohorts were followed by FDG-PET imaging at different time points (34, 47, 55, 62 and 83 days after tumour challenge) and tumour incidence shown by PET, calculated tumour volume and maximum standardized uptake values (SUVmax, see below) as well as survival, were compared between groups.

Histology

Resected tumours and other tissue specimens (spleen, liver, lymph nodes and bone marrow) were fixed in buffered formaldehyde and paraffin-embedded. Haematoxylin and eosin stained sections of all specimens were analyzed.

Immunization procedure

An A20 vaccine was prepared with a lysate obtained by 4 cycles of successive freezing in liquid nitrogen (10 seconds) and thawing at 37°C of a pellet of live A20 cells (3×10^6 per mouse). The pellet was resuspended in PBS buffer and spun down to eliminate cell debris. The supernatant was emulsified volume-per-volume in incomplete Freund's adjuvant (Sigma, Saint Quentin Fallavier, France). A control vaccine was similarly prepared with a lysate of P815 cells. Vaccines (200 µl per mouse) were injected subcutaneously twice in the flanks at a two-week intervals.

Assessment of immune response by enzyme-linked immuno-spot assay (ELISPOT)

To assess the immune response induced by the vaccine, splenocytes from mice vaccinated with either the A20 (9 mice) or the P815 lysate (2 mice) were tested in an *ex-vivo* IFN-γ ELISPOT assay, six days after the last immunization. Briefly, $5x10^5$ splenocytes were incubated 24 h with 10^5 irradiated tumour cells (A20 or P815) in 96 well multiscreen HA plates (Millipore, Guyancourt, France) precoated with an anti-IFNγ antibody (BD-Pharmingen, Erembodegem, Belgium) and revelation of IFNγ-secreting spot-forming cells was performed as previously described [20]. Spots were counted using the KS ELISPOT system (Carl Zeiss SAS, Le Pecq, France).

Micro PET imaging

Serial imaging of mice was performed on a small-animal dedicated micro PET camera (Mosaic, Philips Medical Systems, DA Best, The Netherlands) featuring a circular array of 14,456 gadolinium orthosilicate crystals 2×2×10 mm each. In order to achieve a standardized glycemic state and avoid myocardial uptake, mice fasted for 4 to 12 h before scanning. Image

acquisition was performed one hour after tail-vein injection of an average 4 MBq FDG (full syringe minus empty syringe). Mice were anaesthetized via inhalation of 1-2% isoflurane mixed with oxygen and positioned in the scanner in supine position with continuous inhalation of isoflurane using a dedicated nose device (Minerve, Esternay, France). PET imaging was performed in a three-dimensional mode using one single 10-minute step, the field-of-view of the imager being large enough (11.8 cm) to cover the entire mouse body. Images were reconstructed using an iterative row action maximum likelihood algorithm (RAMLA) after having weighed the mice and calculated the net injected activity for standardized uptake value (SUV) calculation [21]. For each abnormal focus of uptake, an isocontour was drawn semi-automatically (at half-maximum intensity) for the calculation of maximum SUV (SUV_{max}) and tumour volume [22].

Statistical analyses

Statistical analyses were performed using the unpaired two-tailed Student's *t* test with *p* value <0.05 considered significant. Survival was estimated using the product-limit method of Kaplan-Meier and compared using the log-rank test.

Results

In vitro FDG uptake

In vitro assessment of FDG uptake by A20 lymphoma cells was performed to ensure the validity of this cell line for further imaging. As shown on Fig. 1, FDG accumulated rapidly in glucose-deprived A20 cells. Significant uptake was detected as soon as 10 min after contact and increased gradually until 2 hours. Addition of glucose to the buffer consistently hindered FDG uptake which remained faint for the 2 h of the experiment. By contrast, in the control cell population containing the normal B lymphocyte counterpart of the tumour cells, i.e. the spleen cells, FDG accumulated poorly, with little increase over time and was marginally blocked by glucose at the late time points. Thus, A20 lymphoma cells could be used for *in vivo* imaging using FDG-PET.

Clinical and histological features of the A20 lymphoma model

Human large B-cell lymphomas usually develop in secondary lymphoid organs as a single or disseminated disease which extends to bone marrow and blood. When injected subcutaneously, A20 cells proliferated essentially at the injection site (data not shown). Palpable and easily sizeable nodules appeared synchronously in mice and grew rapidly until death. By contrast, after intravenous injection through the tail vein, we observed that A20 lymphoma cells disseminated to mesenteric lymph nodes, liver and spleen. Macroscopic examination showed prominent whitish nodules on the liver surface and dissemination throughout the spleen (Fig. 2a). Depending on their size or location, these lesions caused abdomen enlargement and were generally palpable late in evolution (about one week before death). Histologically, the tumour pattern was characterized by a diffuse homogeneous infiltrate consisting of large and cohesive tumour cells with moderate cytoplasm and pleomorphic nuclei that contained clear chromatin and multiple medium sized nucleoli. There were numerous mitoses admixed with apoptotic bodies and starry-sky histiocytes and focal necrosis was common (Fig. 2b&c). Overall, after intravenous injection of A20 cells, the anatomical sites of development and histological aspect of the disease resembled that of a human large B cell lymphoma, validating the *in vivo* model for PET imaging.

Correlation between PET imaging of tumour lesions and ex-vivo tumour morphology

A pilot experiment in which ten mice were injected with A20 cells and followed by PET at day 42 and 49 was first undertaken (see materials and methods). Visual analysis of the PET

images acquired from these mice confirmed that abnormal foci of uptake corresponded to macroscopic tumours on post-mortem examinations, as shown on Fig. 3 in two representative animals. In mouse-1, the day 42 image showed background physiological uptake by the brain, muscles (principally limbs and neck) and urinary tract. At day 49, a focus of uptake of an estimated 0.04 cm^3 volume was noted on the PET image (iso-intensity contour), that corresponded to a 0.01 cm^3 hepatic tumour nodule at autopsy on the next day. *Ex-vivo* examination revealed a few additional submillimetric hepatic nodules (not visible in photograph) that were not detected by PET. Mouse-2 displayed evidence of significant abdominal tumour burden on the day 42 image, although the tumour was not palpable. The day 49 image showed major growth with large confluent foci of uptake which paralleled the macroscopic aspect of a hepatic nodule cluster. Later in evolution, tumour mass necrosis may eventually result in a focal decrease of FDG uptake (data not shown). Thus, PET images were consistent with tumour growth in all mice and lesions as little as 10 mm^3 could be detected.

Immune response to an A20 cell lysate vaccine in mice

We set up an A20 lymphoma specific vaccination protocol in order to assess the benefits of PET in documenting the vaccine-induced anti-tumour response. A20 cell lysates with adjuvant were injected twice subcutaneously. Induction of a specific anti-A20 cell immune response was first verified. Spleen cells from mice immunized either with A20 or control cell lysates were tested *ex vivo* in an IFN-γ ELISPOT assay (Fig. 4). In mice immunized with control vaccine, no significant response to A20 was detected. An absence of specific response to control cells was also detected in spleens of mice immunized with the A20 vaccine (data not shown). In contrast, the A20-vaccinated mice developed high numbers of IFN-γ secreting T cells in response to A20 cells, demonstrating the efficacy of the immunization procedure for the A20 lymphoma.

Clinical assessment of anti-tumour vaccine efficacy

A20 vaccinated mice (VAC) were challenged intravenously with A20 cells simultaneously with control non immunized (NI) mice. As expected, daily examination of the mice did not allow early discrimination of tumour development between the two groups. Indeed, tumour presence could not be ascertained before the development of voluminous tumour masses that could not be clinically quantified. Therefore, only survival monitoring allowed objective evaluation of tumour protection induced by the vaccine. On day 80, 13% versus 43% of the NI mice and the VAC mice were alive, respectively. These mice were sacrificed at day 130

without evidence of tumour, indicating that the surviving VAC mice durably benefited from the vaccine effect (p=0.043 by Kaplan-Meier analysis, Fig. 5).

Improvement of anti-tumour vaccine efficacy assessment using FDG-PET monitoring

VAC and NI mice were sequentially followed for tumour development by PET at the five time points indicated in Fig. 5. When the first PET series was performed (day 34), all mice were still alive in both cohorts, but two NI mice displayed clinical signs suggesting tumour invasion at examination of the abdomen. PET images indicated lymphoma lesions in the two clinically suspect mice and in two additional NI mice (50% of the NI mice) with total calculated volumes of 1.35, 0.27, 0.11 and 0.10 cm^3 respectively (mean=0.46+/-0.60 cm^3, Fig. 6a). The first two mice died with massive invasion before the scheduled PET image at day 47, while tumours from the latter grew to 5.50 and 5.00 cm^3, respectively. Two additional mice died before next PET acquisition at day 55 and had newly developed bulky lesions at day 47 (2.86 and 2.93 cm^3 respectively). A seventh mouse developed lymphoma later (detection of a 0.35 cm^3 mass at day 55) also with a rapid evolution (not shown).

In contrast, 100% of the VAC mice were free of tumour image at day 34 and 43% had still not developed lymphoma images at days 47, 55 and even later (Fig. 6a and data not shown). In the 4 VAC mice that escaped protection, the first lesions were detected at day 47 i.e. 13 days after first detection in NI mice. In good concordance with expectations, the day 47 tumour volumes were markedly lower in the VAC mice than in the live NI mice (0.68+/-0.48 cm^3 *vs.* 4.073 ± 0.6876 respectively, $p = 0.0034$). Moreover, the tumour activity, which could be quantified by SUV_{max} calculation, was consistently lower in VAC mice than in NI mice, whatever the tumour volume (3.37+/-0.27 vs. 2.11 +/- 0.19 respectively, $p=0.0214$, Fig. 6b), demonstrating lower glucose metabolism in VAC mice tumours.

Overall, the results obtained by PET monitoring demonstrated that the difference in survival between the two mouse cohorts could be anticipated at day 34 and 47 by the number of abnormal FDG foci seen on images and by tumour volume and SUV_{max} calculation, which all indicated delayed lymphoma growth and metabolism in VAC mice.

Discussion

In the present study, we have demonstrated the feasibility and relevance of small animal-dedicated micro PET combined with the FDG radiotracer for the monitoring of tumour growth in the A20 mouse B-cell lymphoma model. In addition, we have highlighted that this technique was able to measure the efficacy of an anti-tumour vaccination procedure, and may therefore be useful in future immunotherapeutic preclinical trials.

The A20 cell line is derived from a spontaneously arising tumour in an aged Balb/c mouse [23]. According to their rapid growth and subsequent increased glucose consumption, A20 cells demonstrated high FDG uptake in preliminary *in vitro* experiments. After intravenous injection in syngeneic mice, the A20 cells massively invaded liver, spleen and abdominal lymph nodes, thus mimicking an aggressive human large B cell lymphoma, in contrast to the usually used subcutaneous models of lymphoma growth [11, 13-17]. This point is essential in the perspective of vaccination since the microenvironment where the tumour develops is thought to play an important role in the quality of the immune response it induces [24, 25].

Intra-abdominal A20 tumour nodules are poorly accessible to clinical examination. Using micro PET, we were able to detect A20 lesions as small as 10 mm^3 in the form of hepatic nodules (see Fig. 3). On the PET image, the volume of this 10 mm^3 nodule was estimated to be 40 mm^3 by the isocontour method, due to the point spread function of the imager. Indeed, despite a spatial resolution of 2 mm, partial volume effects tend to spread the radioactivity around a nodule when its diameter is lower than 2.5 times the resolution [26]. This effect is both responsible for an overestimation of tumour volume and an underestimation of metabolic activity (artificial decrease of the SUV_{max}) in small lesions. However, in many cases, the focus of uptake still remains visible because of the high metabolic activity in the tumour compared to the adjacent physiological background inherent to FDG imaging. Therefore, an excellent correlation was generally observed between images of clinically non palpable tumour lesions and their *ex-vivo* morphology observed macroscopically upon autopsy. This is in accordance with data in humans which demonstrate the great sensitivity of FDG-PET for the detection of occult disease, cancer staging and characterization of morphologically normal masses, particularly in lymphoma [8]. Another pitfall of abdominal tumour imaging with FDG-PET is the physiological bowel uptake that sometimes causes erroneous interpretations in humans, due to peristaltic smooth muscle

contraction or intra-luminal excretion of the tracer [27], but in our studies, we did not encounter such artifacts.

The A20 cell line has been widely used for the *in vivo* testing of vaccination procedures against lymphoma [11-18]. In our study, we vaccinated mice by subcutaneous injections of A20 cell lysate mixed with conventional adjuvant prior to challenge by live A20 cells. This procedure is not applicable to human patients and was used as a model to induce an A20 tumour-specific immune response which was tested by an IFN-γ ELISPOT assay. Comparison of the natural evolution of the vaccinated (VAC) mice and control non immunized (NI) mice revealed significantly better survival of the VAC mice that correlated with a lower incidence and delayed development of lymphoma as visualized by FDG-PET. Most interestingly, FDG-PET allowed early discrimination of tumour growth between the VAC and NI mice. First, day 34 images showed that 50% of the mice had developed tumours in the NI group, whereas all the VAC mice were still tumour-free, suggesting a delay in tumour development in the latter. Second, analysis of the lesions revealed in PET images demonstrated significant differences in volume and SUV_{max} between the two groups (Fig. 6 a and b). These differences revealed a reduced rate of tumour growth in the VAC group. Moreover, the lower SUV_{max} measured in all VAC mice tumours, irrespective of their volume, indicated that they displayed a decreased metabolic activity. Diminished cell viability or proliferation rate have been shown to limit FDG uptake [28, 29]. In VAC mice, the anti-tumour immune response may be responsible for both cell killing by necrosis or apoptosis and cell cycle arrest, a phenomenon known as dormancy [30].

Many FDG-PET studies have been conducted to assess response to chemotherapy in human non-Hodgkin's lymphoma. Cytotoxic treatments alter cellular metabolism before inducing measurable changes in tumour morphology. In agreement with this, FDG-PET predicted therapy response earlier than standard imaging in aggressive lymphoma both in patients and in a chimeric human-mouse Burkitt lymphoma model [1, 2, 31, 32]. Chimeric severe combined immunodefiency (SCID) mice engrafted with human tumour cells and peripheral blood leukocytes are widely used for the preclinical *in vivo* evaluation of new anti-cancer therapies [33]. However, artificial reconstitution of the adaptive immunity and interference of xenogeneic immune responses hamper the study of vaccination-induced anti-tumour responses in this model. To our knowledge, our study is the first to assess the value of FDG-PET for the *in vivo* monitoring of tumour growth following anti-tumour vaccination procedures in immunocompetent mice. To date, survival is the most frequently used end-point, with two major drawbacks: first the need to prolong survival of animals with bulky

tumours and second the poor correlation between survival and total lymphoma tumour burden (e.g. small compressive lesions of the extradural space lead to premature death).

To conclude, we demonstrate that FDG-micro PET is relevant for early detection and follow-up of internal tumours that cannot be detected otherwise by palpation. This functional technique of imaging provides both three dimensional images of tumour location and quantitative parameters (estimated volume and SUV_{max}, [22]), which account for the metabolically active tumour. These parameters are thus determinant for monitoring the efficacy of anti-tumour vaccination procedures and allow an accurate comparison of small animal cohorts. Dynamic observations of tumour development can be obtained from the same individual subject by serial time point image acquisition, as this non-invasive technique is easily performed on anaesthetized mice, thus respecting ethical handling of laboratory animals.

Acknowledgments

This work was supported by the French Association for Cancer Research (ARC grant n° 3257) and by ARTGIL (granted by Amgen and Roche France). C. Chaise was initially supported by a grant from the French ministry for education and research and subsequently from the Fondation pour la Recherche Médicale (FRM). We thank Gaël Grannec and Sandrine Machane for their help with animal care, Dr Fabrice Chrétien for photographs of the animals and Dr William Hempel for careful editing of the manuscript.

References

1. Haioun C, Itti E, Rahmouni A, Brice P, Rain JD, Belhadj K, Gaulard P, Garderet L, Lepage E, Reyes F, Meignan M (2005) [18F]fluoro-2-deoxy-D-glucose positron emission tomography (FDG-PET) in aggressive lymphoma: an early prognostic tool for predicting patient outcome. Blood 105:1376-1381.
2. Spaepen K, Stroobants S, Dupont P, Vandenberghe P, Thomas J, de Groot T, Balzarini J, De Wolf-Peeters C, Mortelmans L, Verhoef G (2002) Early restaging positron emission tomography with (18)F-fluorodeoxyglucose predicts outcome in patients with aggressive non-Hodgkin's lymphoma. Ann Oncol 13:1356-63.
3. Juweid ME, Cheson BD (2005) Role of positron emission tomography in lymphoma. J Clin Oncol 23:4577-80.
4. Czernin J, Weber WA, Herschman HR (2006) Molecular imaging in the development of cancer therapeutics. Annu Rev Med 57:99-118.
5. Yamamoto T, Seino Y, Fukumoto H, Koh G, Yano H, Inagaki N, Yamada Y, Inoue K, Manabe T, Imura H (1990) Over-expression of facilitative glucose transporter genes in human cancer. Biochem Biophys Res Commun 170:223-30.
6. Ido T, Wan CN, Casella JS, et a (1978) Labeled 2-deoxy-D-glucose analogs: 18F labeled 2-deoxy-2-fluoro-D-glucose, 2-deoxy-2-fluoro-D-mannose and 14C-2-deoxy-2-fluoro-D-glucose. J Labeled Compds Radiopharmacol 14:175-183.
7. Sokoloff L, Reivich M, Kennedy C, Des Rosiers MH, Patlak CS, Pettigrew KD, Sakurada O, Shinohara M (1977) The [14C]deoxyglucose method for the measurement of local cerebral glucose utilization: theory, procedure, and normal values in the conscious and anesthetized albino rat. J Neurochem 28:897-916.
8. Burton C, Ell P, Linch D (2004) The role of PET imaging in lymphoma. Br J Haematol 126:772-84.
9. Abbey CK, Borowsky AD, McGoldrick ET, Gregg JP, Maglione JE, Cardiff RD, Cherry SR (2004) In vivo positron-emission tomography imaging of progression and transformation in a mouse model of mammary neoplasia. Proc Natl Acad Sci U S A 101:11438-43.
10. Lyons SK (2005) Advances in imaging mouse tumour models in vivo. J Pathol 205:194-205.
11. Briones J, Timmerman J, Levy R (2002) In vivo antitumor effect of CD40L-transduced tumor cells as a vaccine for B-cell lymphoma. Cancer Res 62:3195-9.

12. Levitsky HI, Montgomery J, Ahmadzadeh M, Staveley-O'Carroll K, Guarnieri F, Longo DL, Kwak LW (1996) Immunization with granulocyte-macrophage colony-stimulating factor-transduced, but not B7-1-transduced, lymphoma cells primes idiotype-specific T cells and generates potent systemic antitumor immunity. J Immunol 156:3858-65.

13. Meziane el K, Bhattacharyya T, Armstrong AC, Qian C, Hawkins RE, Stern PL, Dermime S (2004) Use of adenoviruses encoding CD40L or IL-2 against B cell lymphoma. Int J Cancer 111:910-20.

14. Siegel S, Wagner A, Kabelitz D, Marget M, Coggin J, Jr., Barsoum A, Rohrer J, Schmitz N, Zeis M (2003) Induction of cytotoxic T-cell responses against the oncofetal antigen-immature laminin receptor for the treatment of hematologic malignancies. Blood 102:4416-23.

15. Siegel S, Wagner A, Schmitz N, Zeis M (2003) Induction of antitumour immunity using survivin peptide-pulsed dendritic cells in a murine lymphoma model. Br J Haematol 122:911-4.

16. Zibert A, Balzer S, Souquet M, Quang TH, Paris-Scholz C, Roskrow M, Dilloo D (2004) CCL3/MIP-1alpha is a potent immunostimulator when coexpressed with interleukin-2 or granulocyte-macrophage colony-stimulating factor in a leukemia/lymphoma vaccine. Hum Gene Ther 15:21-34.

17. Rieger R, Kipps TJ (2003) CpG oligodeoxynucleotides enhance the capacity of adenovirus-mediated CD154 gene transfer to generate effective B-cell lymphoma vaccines. Cancer Res 63:4128-35.

18. Curti A, Parenza M, Colombo MP (2003) Autologous and MHC class I-negative allogeneic tumor cells secreting IL-12 together cure disseminated A20 lymphoma. Blood 101:568-75.

19. Passineau MJ, Siegal GP, Everts M, Pereboev A, Jhala D, Wang M, Zhu ZB, Park SK, Curiel DT, Nelson GM (2005) The natural history of a novel, systemic, disseminated model of syngeneic mouse B-cell lymphoma. Leuk Lymphoma 46:1627-1638.

20. Molinier-Frenkel V, Lengagne R, Gaden F, Hong SS, Choppin J, Gahery-Segard H, Boulanger P, Guillet JG (2002) Adenovirus hexon protein is a potent adjuvant for activation of a cellular immune response. J Virol 76:127-35.

21. Graham MM, Peterson LM, Hayward RM (2000) Comparison of simplified quantitative analyses of FDG uptake. Nucl Med Biol 27:647-55.

22. Lee JR, Madsen MT, Bushnel D, Menda Y (2000) A threshold method to improve standardized uptake value reproducibility. Nucl Med Commun 21:685-90.

23. Kim KJ, Kanellopoulos-Langevin C, Merwin RM, Sachs DH, Asofsky R (1979) Establishment and characterization of BALB/c lymphoma lines with B cell properties. J Immunol 122:549-54.

24. Lotze MT, Papamichail M (2004) A primer on cancer immunology and immunotherapy. Cancer Immunol Immunother 53:135-8.

25. Mullins DW, Sheasley SL, Ream RM, Bullock TN, Fu YX, Engelhard VH (2003) Route of immunization with peptide-pulsed dendritic cells controls the distribution of memory and effector T cells in lymphoid tissues and determines the pattern of regional tumor control. J Exp Med 198:1023-34.

26. Hoffman EJ, Huang SC, Phelps ME (1979) Quantitation in positron emission computed tomography: 1. Effect of object size. J Comput Assist Tomogr 3:299-308.

27. Israel O, Yefremov N, Bar-Shalom R, Kagana O, Frenkel A, Keidar Z, Fischer D (2005) PET/CT detection of unexpected gastrointestinal foci of 18F-FDG uptake: incidence, localization patterns, and clinical significance. J Nucl Med 46:758-62.

28. Spaepen K, Stroobants S, Dupont P, Bormans G, Balzarini J, Verhoef G, Mortelmans L, Vandenberghe P, De Wolf-Peeters C (2003) [(18)F]FDG PET monitoring of tumour response to chemotherapy: does [(18)F]FDG uptake correlate with the viable tumour cell fraction? Eur J Nucl Med Mol Imaging 30:682-8.

29. Yamada K, Brink I, Bisse E, Epting T, Engelhardt R (2005) Factors influencing [F-18] 2-fluoro-2-deoxy-D-glucose (F-18 FDG) uptake in melanoma cells: the role of proliferation rate, viability, glucose transporter expression and hexokinase activity. J Dermatol 32:316-34.

30. Uhr JW, Marches R (2001) Dormancy in a model of murine B cell lymphoma. Semin Cancer Biol 11:277-83.

31. Spaepen K, Stroobants S, Dupont P, Van Steenweghen S, Thomas J, Vandenberghe P, Vanuytsel L, Bormans G, Balzarini J, De Wolf-Peeters C, Mortelmans L, Verhoef G (2001) Prognostic value of positron emission tomography (PET) with fluorine-18 fluorodeoxyglucose ([18F]FDG) after first-line chemotherapy in non-Hodgkin's lymphoma: is [18F]FDG-PET a valid alternative to conventional diagnostic methods? J Clin Oncol 19:414-9.

32. Buchmann I, Reinhardt M, Elsner K, Bunjes D, Altehoefer C, Finke J, Moser E, Glatting G, Kotzerke J, Guhlmann CA, Schirrmeister H, Reske SN (2001) 2-(fluorine-

18)fluoro-2-deoxy-D-glucose positron emission tomography in the detection and staging of malignant lymphoma. A bicenter trial. Cancer 91:889-99.

33. Bankert RB, Egilmez NK, Hess SD (2001) Human-SCID mouse chimeric models for the evaluation of anti-cancer therapies. Trends Immunol 22:386-93.

Figure legends

Fig. 1: ***In vitro FDG uptake***. Comparison of *in vitro* FDG uptake by A20 lymphoma cells (a) and control splenocytes (b), in PBS alone (gray bars) and PBS+competitor glucose (white bars). Data are expressed as % FDG uptake as defined by Eq. 1. Data shown are representative of two independent experiments.

Fig. 2: ***A20 lymphoma cell infiltration of mouse liver and spleen after intravenous injection.***

A Balb/c mouse injected in the tail vein with 10^5 A20 cells was sacrificed 49 days later when displaying bulky abdominal palpable lesions. Spleen and liver were compared to corresponding organs from a normal mouse (a). The histologic aspect of the A20 infiltrate in the liver is depicted in panels b and c. Similar aspects were observed in spleen, lymph nodes and bone marrow.

Fig. 3: ***Correlation of FDG uptake and ex-vivo tumour morphology.***

Mice were injected in the tail vein with A20 cells and sacrificed 50 days later. PET images acquired on day 42 and day 49 respectively, and macroscopic aspects of the abdomen on day 50 are shown side by side for two representative mice out of 10. In mouse 1 (upper row), the blue arrow indicates a small hepatic lesion visible on the day-49 PET image. In mouse 2 (lower row), the blue arrow indicates a massive hepatic invasion and its progression at a one-week interval.

Fig. 4: ***Anti-A20 immune response induced by vaccination.*** Splenocytes from mice vaccinated with an A20 or P815 control lysate (9 and 2 mice respectively) were taken six days after the last vaccine injection and tested ex-vivo in an IFN-γ ELISPOT assay against A20 and P815. Data are expressed as the number of IFN-γ secreting cells from one representative mouse per vaccine (mean +/- SD of triplicate test).

Fig. 5: ***Comparison of survival curves between vaccinated and control mice after simultaneous tumour challenge***.

A statistically significant difference is shown by Kaplan-Meier analysis. The dates of PET examinations on day 34, 47, 55, 62 and 83 during the follow-up are shown by the vertical dotted lines.

Fig. 6: ***Tumour volume and SUV_{max} measured on PET images in vaccinated and control mice.***

(a) Record of tumour-free mice, dead mice and total tumour volume for tumour-bearing mice. The FDG-PET time course (days 34, 47 and 55) post-tumour challenge in NI (n=8, black dots) and VAC mice (n=7, white dots) is indicated. Lymphoma development was delayed in VAC mice (Student's t test at day 47: p = 0.0034). (b) Maximum standard uptake values (SUV_{max}) as a function of tumour volume. All the data acquired on days 34, 47 and 55 are shown, i.e. the same mouse can be represented twice. SUV_{max} were significantly lower in VAC mice than in NI mice (Student's t test: p = 0.0214).

Fig. 1

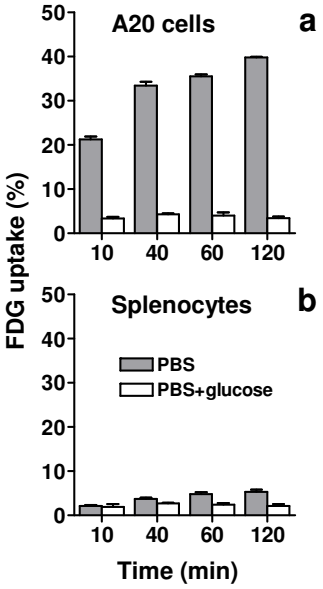

1

2

Fig. 2

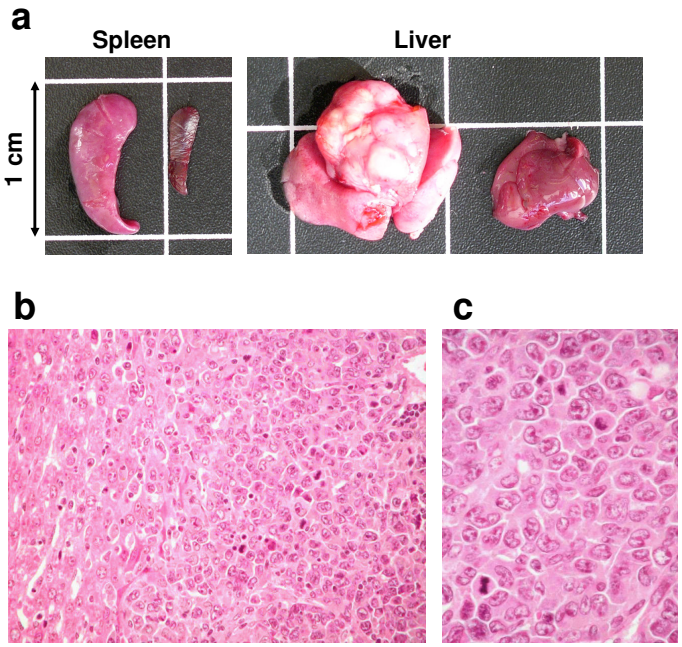

3

Fig. 3

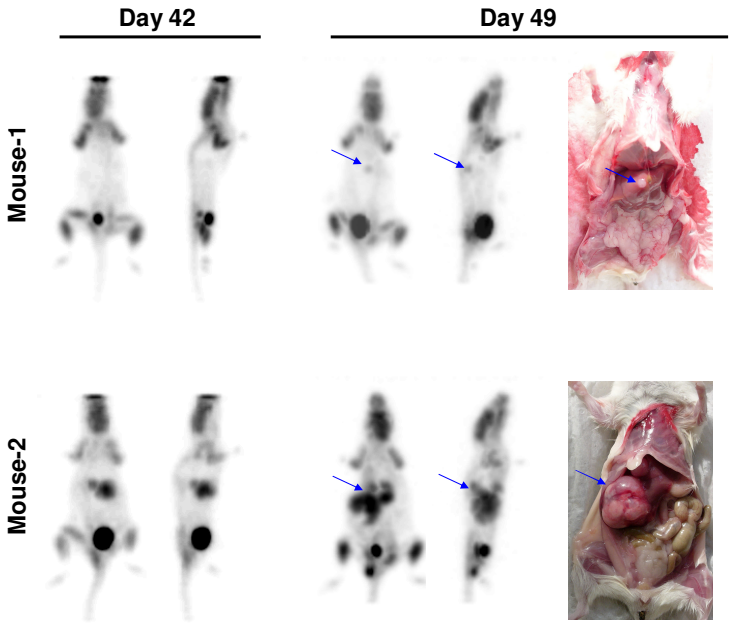

1
2

Fig. 4

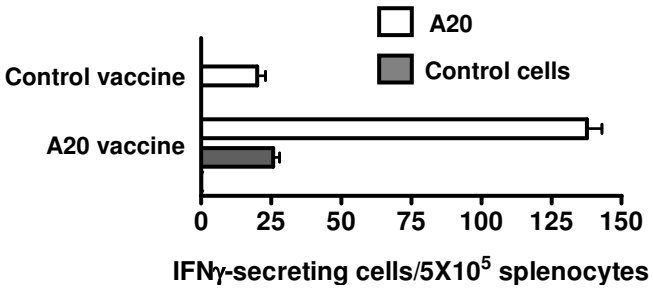

3

Fig. 5

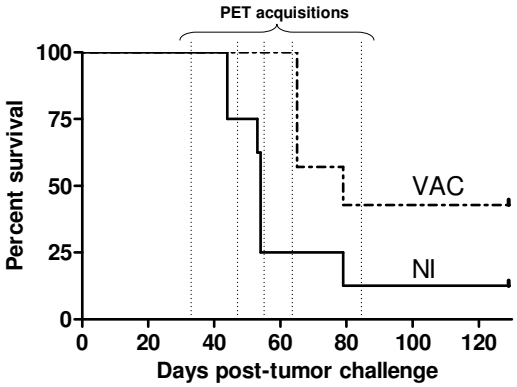

1

2

Fig. 6

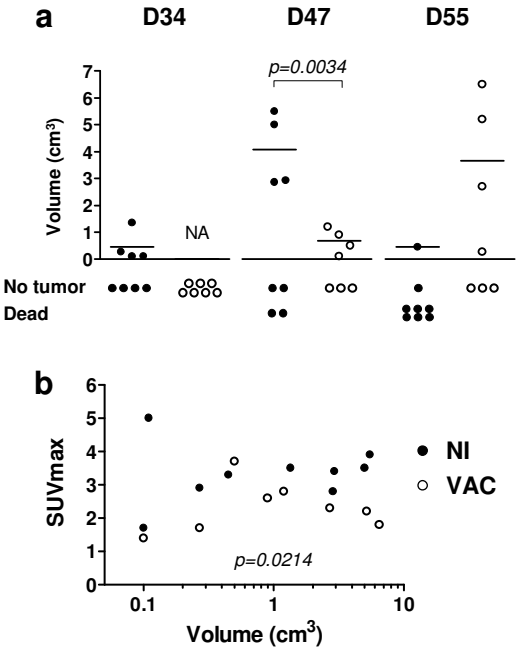

3